POLYOXOMETALATES

Open Access
RESEARCH ARTICLE

Expanding polyoxopalladate diversity: Ce^{4+}-containing structures and chiral lanthanide clusters

Zoë L. Sinclair, Vishal Lakhanpal, De-Liang Long ✉, Nicola L. Bell, and Leroy Cronin ✉

School of Chemistry, University of Glasgow, Glasgow G12 8QQ, UK

Cite This: *Polyoxometalates*, **2026**, *5*, 9140137

Read Online

ABSTRACT: The incorporation of lanthanides into polyoxometalates (POMs) is a fascinating area of research due to their unique chemical and physical properties, as well as their potential applications. Polyoxopalladate (POP) clusters feature flexible central cavities and coordination geometries dictated by their central metal ion templates and external capping groups. Two primary structure types have been reported: $\{Pd_{12}\}$ cubes and $\{Pd_{15}\}$ stars, which can accommodate various central metal ions, ranging from common transition metals in the +2 oxidation state to less conventional lanthanides in the +3 oxidation state. This work explores POP clusters containing cerium ions, leading to the discovery of two new structure types: $[CePd_{13}O_9(SeO_3)_9(H_2O)]^{6-}$ (**1**) and $[Ce_3Pd_{22}O_{16}(SeO_3)_{16}]^{8-}$ (**2**). Cluster **1** adopts a fused "star-cube" structure, combining half $\{Pd_{15}\}$ star and half $\{Pd_{12}\}$ cube with Ce^{4+} as the central template. **2** exhibits a twisted dumbbell-shaped structure (D_{2d} symmetry), where two Ce^{4+}-centred $\{CePd_{11}\}$ cubes are bridged by a third Ce^{4+} ion at the cluster core. Parallel experiments with other lanthanides yielded two propeller-like chiral POPs $[LnPd_{12}O_7(SeO_3)_8Cl(H_2O)_2]^{4-}$ (Ln = Eu^{3+} (**3**); Ln = Gd^{3+} (**4**)), both displaying C_3 symmetry. Notably, this represents one of the rare instances in POP chemistry where a capping ligand (SeO_3^{2-}) directly coordinates to the central lanthanide ions (Eu^{3+} and Gd^{3+}). The twisted coordination of this capping ligand induces a uniform tilt in a set of $\{PdO_4\}$ planes, resulting in the clusters' propeller-like chirality. In contrast, similar reaction conditions for Tb^{3+} produced $[TbPd_{12}O_8(SeO_3)_8]^{5-}$ (**5**), a normal cubic structure.

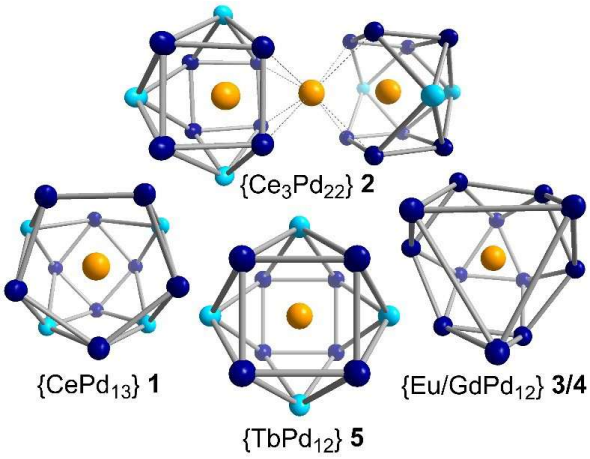

KEYWORDS: polyoxopalladate, lanthanide, selenite, palladium, Ce^{4+} oxidation state, chiral cluster

1 Introduction

Palladium compounds are of significant commercial interest due to their widespread use in catalytic processes [1, 2]. Polyoxopalladates (POPs) [3] are well-defined molecular structures composed of Pd^{2+} centres in a square-planar $\{PdO_4\}$ coordination geometry. Under weakly acidic conditions, the condensation reaction of these units in the presence of heteroanions (e.g. PO_4^{3-}, $PhAsO_3^{2-}$ and SeO_3^{2-}) leads to the assembly of diverse POP architectures (Fig. 1). Since 2008, POP structures such as cubes, stars, disks, dumbbells, wheels, and open-shell frameworks have been reported [4–9]. These clusters exhibit remarkable stability in both solid and solution states, in both aqueous and organic solvents. Their chemical diversity, structural versatility, and straight forward synthesis make them ideal candidates for studying catalytic mechanisms and developing advanced catalytic materials [10].

A key feature of POP chemistry is the role of heteroanions, which are essential for cluster formation, stabilization, and anionic charge. Unlike the interior templating heteroanions in traditional Mo and W polyoxometalates (POMs) [11], the heteroanions in POPs coordinate to Pd atoms from outside the clusters as exterior capping-groups. They generally follow the formula RXO_3^{n-}, where X is a Group 15 or 16 element (e.g., P, As, Sb, S, Se, and Te), whilst R can be an organic group (e.g., Ph in $PhAsO_3^{2-}$) [11], an oxo group (forming tetrahedral XO_4^{n-} anions like PO_4^{3-}), or a lone pair (e.g., SeO_3^{2-}). A representative coordination model of capping-groups can be viewed in cubic clusters $\{Pd_{13}(RXO_3)_8\}$, where RXO_3 = AsO_4^{3-} [4], $PhAsO_3^{2-}$, and SeO_3^{2-} [12]. Three oxygen atoms each bind to a Pd atom at the cube corner.

POPs exhibit a wide range of architectures, including rare large structures like ring-shaped $\{Pd_{84}\}$ [7, 13], $\{Pd_{72}\}$ [14], and disk-like $\{Pd_{40}\}$ [15] (Fig. 1). However, most small POPs belong to two fundamental structure types: M-centred cube $\{MPd_{12}\}$ and M-containing star $\{M_nPd_{15}\}$, where M can be Pd itself (e.g., $\{Pd_{13}\}$ [6]

Received: February 23, 2026; **Revised:** May 6, 2026
Accepted: May 20, 2026

✉Address correspondence to De-Liang Long, deliang.long@glasgow.ac.uk; Leroy Cronin, lee.cronin@glasgow.ac.uk

https://doi.org/10.26599/POM.2026.9140137

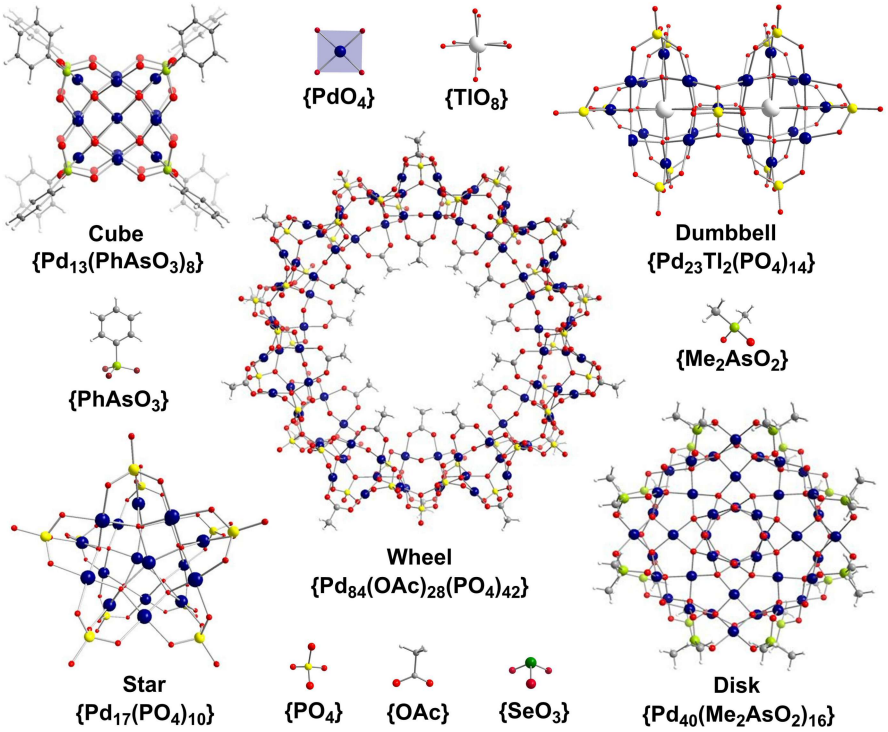

Figure 1 Representative structure types and building blocks for POPs. Colour scheme: Pd blue, Tl white, As/Se green, P yellow, O red, C and H gray.

and $\{Pd_{17}\}$ [16]) (Fig. 1) or heterometals from across the periodic table (with n = 1 or 2 for $\{M_nPd_{15}\}$). The $\{MPd_{12}\}$ cube (Fig. 2(a)) resembles a rectified square prism represented by a blue cube and four side-facing Pd atoms in cyan. The $\{Pd_{15}\}$ star (Fig. 2(b)) can be described as a rectified pentagonal-prism, a blue coloured pentagonal prism and five side-facing Pd atoms in cyan. The first cube structure, $[Pd^{II}_{13}As^{V}_{8}O_{34}(OH)_6]^{8-}$ ($\{Pd_{13}As_8\}$), was synthesised in 2008 [4]. Subsequent studies revealed that the central Pd^{2+} (in an irregular $\{PdO_8\}$ environment) can be replaced by other main-group or transition metal ions, forming $\{MPd_{12}\}$ cubes. The star-shaped $[Pd_{0.4}Na_{0.6}\subset Pd_{15}P_{10}O_{50}H_{6.6}]^{12-}$ ($\{Pd_{15}P_{10}\}$) [5] features a cavity that can accommodate up to two Pd atoms, depending on the synthesis conditions [16]. In many other cases, the cavity holds a single ion of other elements [17] in the periodic table (Fig. 2(b)).

The incorporation of lanthanides into POPs was first reported in 2010, where the central Pd^{2+} in $\{Pd_{13}L_8\}$ was replaced with Ln^{3+}, yielding $\{LnPd_{12}L_8\}$ (L = $PhAsO_3^{2-}$) [18]. The work explored the structural and electronic flexibility of POPs by introducing lanthanides, which impact unique luminescent and magnetic properties to POMs [19–24]. Recently, $[CePd_{12}O_8(AsO_4)_8]^{12-}$ (with Ce^{4+}) was reported [25], further expanding the scope of lanthanide-POP chemistry.

We initially aimed to incorporate Ce^{3+}/Ce^{4+} into POPs, establish a robust synthetic protocol, and explore the formation of large architectures akin to $\{Pd_{84}\}$ [13, 26]. Single-crystal X-ray diffraction was employed for unit-cell screening and full structure determination. Early experiments yielded a novel Ce^{4+}-containing POP, $[CePd_{13}O_9(SeO_3)_9(H_2O)]^{6-}$ (**1**). Subsequent screening of hundreds of reactions under varied conditions revealed several new lanthanide-POPs, including the twisted dumbbell-shaped $[Ce_3Pd_{22}O_{16}(SeO_3)_{16}]^{8-}$ (**2**). Rational substitution of Ce with other lanthanides produced two propeller-like chiral POPs $[LnPd_{12}O_7(SeO_3)_8Cl(H_2O)_2]^{4-}$ (Ln = Eu^{3+} (**3**); Ln = Gd^{3+} (**4**)) of C_3 symmetry and the cubic $[TbPd_{12}O_8(SeO_3)_8]^{5-}$ (**5**).

2 Results and discussion

2.1 Chemistry of Ce^{4+}-containing POMs

Tetravalent cerium (Ce^{4+}) compounds are valuable reagents in organic synthesis, oxidizing agents, and oscillating reactions. Cerium is among the few lanthanides that can form stable compounds in the +4 oxidation state, a property attributed to its $4f^0$ electronic configuration. The Ce^{3+}/Ce^{4+} redox pair is well-documented and advantageous due to its long-team stability, thermal resistance, colorless nature (facilitating titration measurements), and highly positive standard redox potential [27]. Despite its broad applications, Ce^{4+} remains rare in POM chemistry [28–33]. Kortz et al. reported a cubic POP cluster $\{Pd_6Ce_8(Me_2AsO_2)_{16}\}$ [34] featuring eight Ce^{4+} ions at the cube vertices and six Pd^{2+} at cube face centers. Most recently they described a Ce^{4+}-centred cube structure, $[CePd_{12}O_8(AsO_4)_8]^{12-}$ [25]. The +4 oxidation state can be accessed by simple aerial oxidation of an alkaline Ce^{3+} solution at room temperature [35]. Solution studies indicate that Ce^{4+} exists as an oxo-bridged dimer, which may participate in oxidation reactions [36, 37]. We hypothesised that increasing the pH would favor the Ce^{3+} oxidation, leading to $Ce(OH)_4$ formation rather than $Ce(OH)_3$. The latter only forms at very high pH (> 10), which is typically incompatible with POM synthesis (except for polyoxoniobates). Thus, a moderately alkaline pH should promote $Ce(OH)_4$ formation [38]. Given that nearly all reported lanthanide-POP clusters feature trivalent lanthanides in the $\{MPd_{12}L_8\}$ cube structure, we proposed that stabilizing Ce^{4+} could enable the formation of novel POP topologies, potentially through intermediate species.

2.2 Synthesis

Compounds **1** and **2** were obtained by using Ce^{3+} as starting materials. Through pH adjustment, heating and prolonged

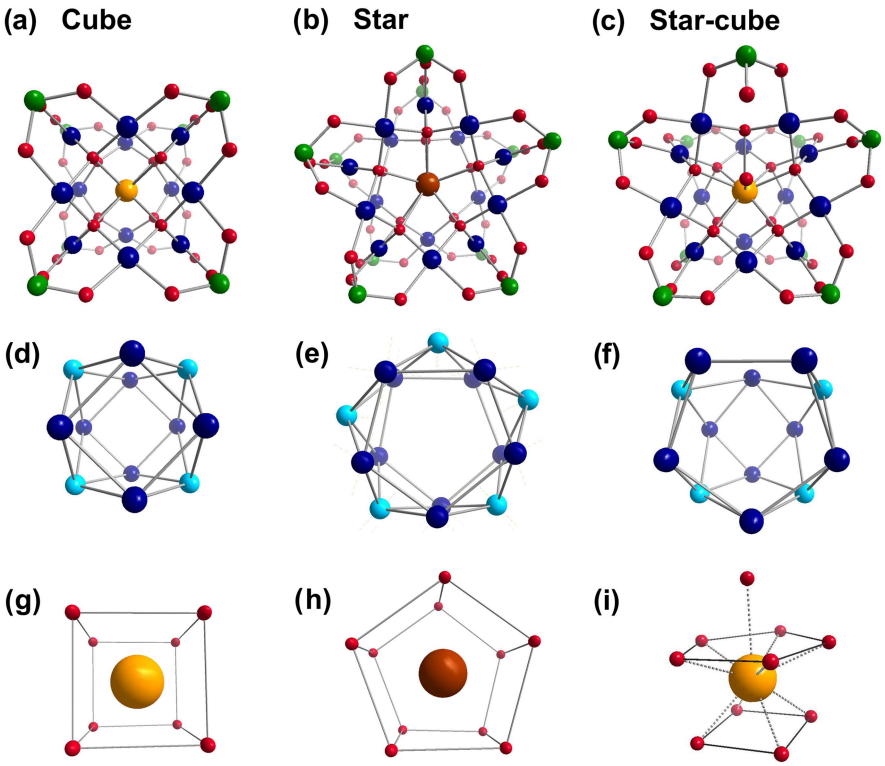

Figure 2 For comparison, representative POP structures: (a) cube $\{MPd_{12}O_8(XO_3)_8\}$ and (b) star $\{MPd_{15}O_{10}(XO_3)_{10}\}$, and (c) the new starcube $[CePd_{13}O_9(H_2O)(SeO_3)_9]^{6-}$ (**1**). Arrangements of palladium atoms are respectively shown below the structures: (d) cube (blue) plus four side face addendums (cyan), (e) pentagonal prism (blue) plus five addendums (cyan), and (f) pentagon-square cylinder (blue) plus four side face addendums (cyan). Coordination spheres of central M/Ce atom: (g) eight coordinated MO_8 as cube, (h) ten coordinated MO_{10} as pentagonal prism, and (i) ten coordinated MO_{10} as irregular polyhedron. Color scheme: Ce/M yellow/orange, Pd blue/cyan, Se/X green, O red.

crystallization, Ce^{3+} was oxidised to Ce^{4+} and subsequently encapsulated within POP clusters. Similar Ce(III) → Ce(IV) oxidation processes have been documented in Refs. [25, 34]. The Ce^{4+} oxidation state was verified by bond valence sum (BVS) calculations (Table S1 and S2 in the Electronic Supplementary Material (ESM)), using established parameters [39] for both Ce^{3+} and Ce^{4+}. In both compounds, the BVS results for Ce were consistent with the +4 oxidation state.

Compound **1** was synthesised by referring the synthetic procedure for producing $[Pd^{II}_{13}Se^{IV}_{8}O_{32}]^{6-}$ ($\{Pd_{13}Se_8\}$) [12]. The reaction mixture solution displayed quite acidic pH, pH 4.1–4.3, due to the addition of $CeCl_3$. To achieve a more neutral pH of 6.4, NaOH was added slowly under vigorous stirring. The pH adjustment required careful monitoring, as Ce^{3+} ions can readily precipitate as $Ce_2O_3{\cdot}6H_2O$ [22], a process reversible only through H^+ addition. This was undesirable, as POM formations are sensitive to repeated pH adjustment and to solution volume. Following pH optimization, the solution was heated with vigorous stirring. The resulting unreacted materials and precipitates, being too fine for paper filtration, were separated by centrifugation. The supernatant was carefully pipetted into a fresh glass vial and stored at 18 °C for crystallisation. The solutions were monitored over several weeks, with notable changes observed. An initial orange precipitate formed during early stages. The solution was decanted from this precipitate and transferred to a new vial to continue crystallisation. After three weeks, very fine dark red needles appeared in some vials; however, attempts to analyse them via single-crystal X-ray diffraction were unsuccessful due to their fragility and small size. After an additional three weeks, larger and more robust dark red needles formed (Fig. S1 in the ESM), which were suitable for structural analysis.

Compound **2** was initially identified in a crystallisation of 9 months (left in COVID19 lockdown period), a timeframe impractical for reproducible research. To develop a more efficient synthesis, we conducted a systematic investigation of synthetic parameters. We examined a matrix of conditions varying sodium acetate buffer concentrations (0.1, 0.2, 0.3, 0.4, 0.5, 0.8, 1.0, 2.0, and 3.0 M) with each concentration tested under eight different combinations of temperature (room temperature and 80 °C), cerium chloride quantity (0.028 and 0.056 mmol), and selenium dioxide amount (0.315 and 0.631 mmol). Each condition was duplicated, resulting in 16 reactions per buffer concentration and 144 reactions in total. For operational efficiency, stock solutions of cerium chloride and selenium dioxide were prepared in sodium acetate buffer, which served as the reaction medium. Solid palladium acetate was added to individual vials followed by the stock solutions. After pH adjustment with NaOH, reactions were stirred at either room temperature or 80 °C for one hour before filtration. This comprehensive exploration of chemical space successfully yielded high-quality crystals of compound **2**, within just three weeks, a significant improvement over the original 9-month period. The optimal conditions for compound **2** formation employed 0.028 mmol Ce^{3+} and 0.315 mmol SeO_2 and an 80 °C reaction temperature, though crystallization occurred successfully across a sodium acetate concentration range of 0.3–1.0 M. The synthetic procedure closely resembled that of compound **1**, differing primarily in buffer concentration. Interestingly,

compound **1** formed as a side product under certain synthetic conditions of compound **2**. Microscopic examination (Fig. S2 in the ESM) revealed large, deep-red compound **2** crystals alongside thin needle-like compound **1** crystals and small red cubic crystals of $\{Pd_{13}Se_8\}$ [12], with all phases confirmed by single-crystal X-ray diffraction unit cell determinations.

Following the successful isolation of Ce^{4+}-containing compounds, **1** and **2**, we expanded our investigation to incorporate other lanthanides. Employing a similar synthetic protocol but substituting Eu^{3+}, Gd^{3+} and Tb^{3+} chloride salts, we targeted mid-to-late lanthanides to examine the effects of varying ionic radii and oxidation states. Under comparable reaction conditions, the Eu and Gd systems yielded isostructural propeller-like chiral clusters (**3** and **4**, respectively), while the Tb system produced a conventional cubic structure (**5**).

2.3 Structure determinations

All compounds obtained were characterised by single-crystal X-ray diffraction. Crystal data and refinement details are listed in Table 1. Pd centres were identified by their characteristic square planar $\{PdO_4\}$ coordination with Pd–O bond distances of ~ 2.0 Å. Lanthanide atoms were found in high coordination numbers (8–10), with Ln–O bond distances averaging 2.5 Å. Se atoms adopt triangular pyramidal $\{SeO_3\}$ geometry (Se–O ~ 1.7 Å). Na atoms were recognised outside clusters with Na–O distances of ~ 2.4 Å. Solvated water molecules were found mostly with partial occupancy. The SQUEEZE procedure [40] was employed to evaluate solvent-accessible volumes and number of electrons. Compound formulae were determined through structure refinement, with sodium and solvent water content adjusted based on charge balance and SQUEEZE results.

$[CePd_{13}O_9(SeO_3)_9(H_2O)]^{6-}$ (**1**), crystallising in the form of $Na_6[CePd_{13}O_9(SeO_3)_9(H_2O)](H_2O)_{20}$ ($\{Pd_{13}Se_9\}$) (Fig. S3 in the ESM), represents a significant topological advance in POP chemistry as the first example combining features of both cube and star geometries. As depicted in Fig. 2, while known $\{Pd_{12}\}$ cubes adopt a rectified square prism arrangement of palladium atoms (Fig. 2(d)) and $\{Pd_{15}\}$ stars adopt a rectified pentagonal prism (Fig. 2(e)), cluster **1** $\{Pd_{13}\}$ features a mixture of a half cube and half star (Fig. 2(f)). This novel arrangement maintains only four side-facing Pd atoms, with the back portion resembling a square (cube-like) and the front forming a pentagon (star-like). **1** encapsulates a cerium ion in +4 oxidation state at the cluster centre, one of the few POPs containing a lanthanide ion in +4 oxidation state referring to recent report of $[CePd_{12}O_8(AsO_4)_8]^{12-}$ [25]. The central Ce^{4+} with oxidation state confirmed by BVS (Table S1 in the ESM) coordinates to 10 oxygen atoms: five from the half star portion, four from the half cube region, plus one additional oxygen from a terminally bound water molecule that extends outward along the cluster's central axis (Fig. 2(i)). All Pd^{2+} centres exhibit the expected square-planar coordination geometry and eight SeO_3^{2-} capping groups adopt trigonal pyramid geometry with their stereochemically active lone pairs pointing outwards. Each SeO_3^{2-} capping group is located on the front faces of one of the triangles of the rectified square/pentagonal prism. The ninth SeO_3^{2-} exhibits a μ_2 bridging mode linking only two Pd centres. This Se atom is disordered over two positions (Se5 and Se5' in Fig. S4 in the ESM) with associated oxo terminals hanging on the opposite sides of these disordered positions, but the major portion undergoes hydrogen bonding with the Ce-bound water molecule.

Table 1 Crystal data and structure refinement for **1**–**5**

	1	**2**	**3**	**4**	**5**
Empirical formula	$CeH_{42}Na_6O_{57}Pd_{13}Se_9$	$Ce_3H_{36}Na_8O_{82}Pd_{22}Se_{16}$	$ClEuH_{52}Na_4O_{57}Pd_{12}Se_8$	$ClGdH_{52}Na_4O_{57}Pd_{12}Se_8$	$H_{20}Na_5O_{42}Pd_{12}Se_8Tb$
Formula weight	3326.23	5556.73	3152.26	3157.55	2874.51
Crystal system	Orthorhombic	Cubic	Orthorhombic	Orthorhombic	Cubic
Space group	*Pbcm*	$P2_13$	$P2_12_12_1$	$P2_12_12_1$	$Pm\bar{3}$
a (Å)	14.9146(3)	30.6636(4)	13.2291(3)	13.2620(4)	15.1224(4)
b (Å)	20.8988(4)	30.6636(4)	23.8071(6)	23.7505(10)	15.1224(4)
c (Å)	19.0841(3)	30.6636(4)	41.7111(10)	41.6589(13)	15.1224(4)
Volume (Å^3)	5948.46(19)	28831.6(11)	13136.8(5)	13121.7(8)	3458.3(3)
Z	4	12	8	8	3
ρ (calculated) (g·cm^{-3})	3.714	3.840	3.188	3.197	4.141
μ (mm^{-1})	10.244	11.595	8.747	8.811	12.540
F(000)	6104	30,120	11,648	11,656	3900
Θ range (°)	2.222 to 25.999	2.485 to 25.992	2.353 to 25.705	2.257 to 25.392	2.333 to 25.960
Reflections collected	120,807	59,345	161,298	494,774	8204
Unique reflections	6031	18,546	59,567	24,060	1279
R(int)	0.1021	0.0852	0.1631	0.3968	0.0791
Data/restraints/parameters	6031/0/411	18,546/66/1085	59,567/115/1326	24,060/210/1269	1279/6/93
R_1 and R_2 ($I>2\sigma(I)$)	0.0567, 0.1033	0.0485, 0.0964	0.0890, 0.1685	0.0971, 0.2258	0.0418, 0.0908
R_1 and wR_2 (all data)	0.0659, 0.1062	0.0813, 0.1068	0.1695, 0.1987	0.1466, 0.2587	0.0642, 0.0986
Goodness-of-fit on F^2	1.275	1.013	0.971	1.031	1.046
Flack parameter	—	0.015(7)	0.431(7)	0.04(3)	—
Largest diff. peak and hole/e Å^{-3}	1.39 and −1.02	1.503 and −0.88	2.05 and −1.34	3.66 and −1.34	2.80 and −2.63
CCDC number	2385249	2385250	2385251	2385252	2385253

$[Ce_3Pd_{22}O_{16}(SeO_3)_{16}]^{8-}$ (**2**), crystallising in the form of $Na_8[Ce_3Pd_{22}O_{16}(SeO_3)_{16}](H_2O)_{18}$ ($\{Ce_3Pd_{22}Se_{16}\}$) (Fig. S5 in the ESM), adopts a dumbbell shaped structure that differs significantly from previously reported $\{Cu_2Pd_{22}P_{12}\}$ [41], $\{Na_2Pd_{22}As_{15}\}$ [42], and $\{Tl_2Pd_{23}P_{14}\}$ [43] (Fig. 1). Whilst these known structures all possess D_{2h} symmetry with a horizontal mirror plane relating the two dumbbell halves, $\{Ce_3Pd_{22}Se_{16}\}$ (**2**) exhibits a D_{2d} symmetry where two $\{CePd_{11}\}$ cube units are related by an improper 4-fold axis, resulting in a twisted dumbbell. These two lacunary $\{CePd_{11}\}$ cube (missing one side-facing Pd^{2+} compared to the standard $\{Pd_{12}\}$ cube), each containing a Ce^{4+} template ion, are joined together through a third Ce^{4+} ion at the cluster centre (Fig. 3 and Fig. S5 in the ESM). This central Ce^{4+} ion connects two $\{CePd_{11}\}$ lacunary cubes through four μ_2-O atoms each from a SeO_3^{2-} capping group, and four μ_4-O atoms that in the $\{CePd_{11}\}$ cube. The central Ce^{4+} induces the distinctive twist by requiring its four SeO_3^{2-} ligands to adopt a staggered arrangement, forcing a 90° rotation between the two $\{CePd_{11}\}$ units. This is a special feature of the big Ce^{4+} ion, acting as a linker, that connects two $\{Pd_{11}\}$ units, different from Cu^{2+}, Na^+ and Pd^{2+} as linkers in $\{Cu_2Pd_{22}P_{12}\}$ [41], $\{Na_2Pd_{22}As_{15}\}$ [42], and $\{Tl_2Pd_{23}P_{14}\}$ [43]. BVS calculations confirm the tetravalent state of all three Ce centres (Table S2 in the ESM), consistent with the formation mechanism involving pH-dependent air oxidation of Ce^{3+} precursors observed for **1**.

$[LnPd_{12}O_7(SeO_3)_8Cl(H_2O)_2]^{4-}$ (Ln = Eu (**3**) and Gd (**4**), Figs. S6 and S7 in the ESM) crystallise in the form of $Na_4[LnPd_{12}O_7(SeO_3)_8Cl(H_2O)_2](H_2O)_{24}$. **3** and **4** are isostructural and both have a unique chiral symmetry of C_3 point group, representing the first examples of chiral POPs. The unique chirality arises from twisting coordination of a distinctive SeO_3^{2-} capping group positioned on the C_3 axis (highlighted by cyan Se–O and Pd–O bonds in Fig. S8 in the ESM). This particular SeO_3^{2-} group exhibits two remarkable features: (1) It coordinates directly to the central lanthanide ions (Eu^{3+} or Gd^{3+}), representing one of the rare instances where a capping anion binds to the central hetero metal in POP chemistry; and (2) it bridges three palladium centres, each of which additionally coordinates to a terminal ligand (either a water molecule or a Cl^- ion in a 2:1 occupancy ratio, see Fig. S9 in the ESM). In all previously known POPs, Pd ions bind to a capping group and not a terminal ligand. The central lanthanide ion (Eu^{3+} or Gd^{3+}) achieves ten-coordination through interactions with seven μ_4-O oxo ligands that join Pd ions and the three oxo atoms from the aforementioned unique SeO_3^{2-} group (Fig. S10 in the ESM). The twelve palladium atoms maintain their characteristic square-planar coordination geometry but arrange in a distorted truncated cuboid framework (Fig. S12 in the ESM). While nine palladium centres follow the conventional POP coordination pattern (bridged by two μ_4-O and two SeO_3^{2-} oxygen atoms), the remaining three show an unusual coordination environment. These three Pd centres each bind to: one μ_4-oxo, one terminal oxygen, one oxygen from a standard SeO_3^{2-} group, and one oxygen from the unique twisted SeO_3^{2-} ligand. This asymmetric coordination causes the three $\{PdO_4\}$ units (highlighted with blue squares in Fig. 4) to tilt towards uniformly in a propeller-like fashion (Fig. S8 in the ESM). The propeller blade angles are in the range 72°–81°, see Figs. S6 and S7 in the ESM captions for more details. Although individual crystals demonstrate clear chirality, bulk samples exist as a racemic conglomerate. The absolute configuration can be assigned using standard chiral nomenclature (−)-M and (+)-P, following conventions for axially chiral compounds [44].

Previous work by Kortz and colleagues has demonstrated the incorporation of all lanthanide ions into cubic $\{Pd_{12}\}$ cages using various capping ligands SeO_3^{2-}, AsO_4^{3-}, $PhAsO_3^{2-}$, and $PhPO_3^{2-}$ [18, 25, 45, 46]. The cavity size accommodating the heterometal ions shows slight variability, as evidenced by the Ln–O distances in cubic $\{LnO_8\}$ environments decreasing smoothly from La–O (2.458 Å) to Lu–O (2.303 Å), following the lanthanide contraction trend. A notable exception is the $\{CePd_{12}\}$ [25] structure, where the Ce–O distance (2.343 Å) significantly deviates from this trend due to the Ce^{4+} oxidation state. These observations demonstrate that the cubic POP framework exhibits modest flexibility to accommodate the coordination requirements of encapsulated lanthanide ions, confirmed by computational methods [46]. To assess the potential for incorporating other lanthanides into our newly discovered structural types—the star-cube $\{CePd_{13}\}$ (**1**) and chiral propeller $\{GdPd_{12}\}$ (**4**), we carried out

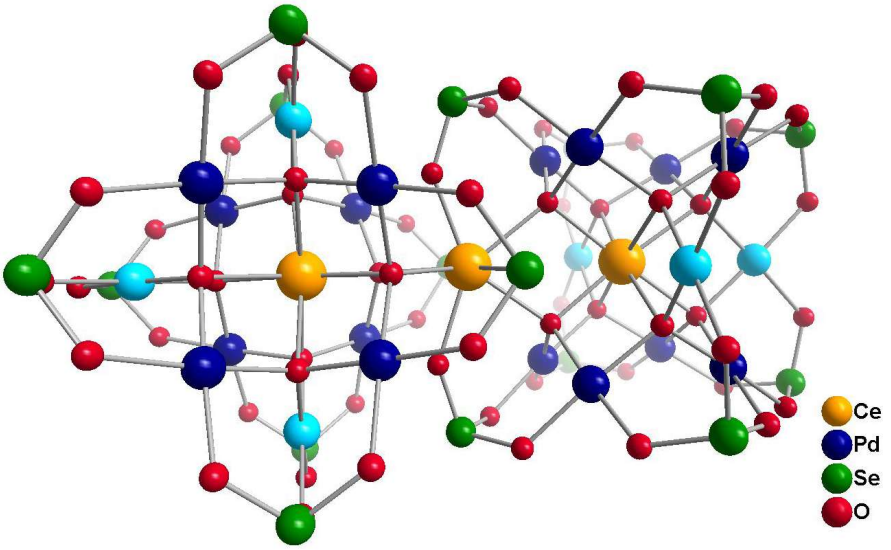

Figure 3 Structure of $[Ce_3Pd_{22}O_{16}(SeO_3)_{16}]^{8-}$ (**2**): Pd cube (blue) plus three side face Pd addendums (cyan) for each $\{CePd_{11}\}$ cubic unit. The middle Ce atom (yellow) is located on one of the side face addendum positions jointing two $\{CePd_{11}\}$ cubic units. Related to each other, the two $\{CePd_{11}\}$ cubes twist 90° along the molecule long axis with references of side face addendums (cyan).

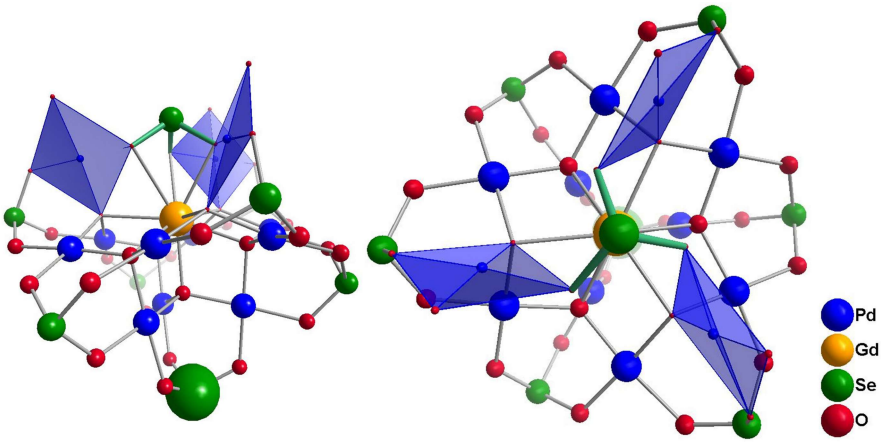

Figure 4 Structure of the cluster $[GdPd_{12}O_7(SeO_3)_8Cl(H_2O)_2]^{4-}$ (**4**): left, side view; right, top view along the molecular C_3 symmetric axis. The unique SeO_3 ligand that directly coordinates to Gd is highlighted with green Se–O bonds. Three $\{PdO_4\}$ units highlighted with blue squares tilt towards uniformly like propeller due to twisting coordination of the unique capping SeO_3 ligand. The propeller blade angles are in the range 72°–81°, see Figs. S6 and S7 in the ESM for more details.

empirical BVS calculations by assuming alternative lanthanides at the Ce and Gd positions (Table S6 in the ESM). For comparative analysis, we also examined the $\{NaPd_{15}\}$ [4] structure (Fig. 2(b)) as a model system, evaluating lanthanide substitution at the central sodium site. The calculations for $\{Pd_{15}\}$ cage reveal substantial BVS deviations for all lanthanides, suggesting its cavity is too large to efficiently accommodate these ions, making $\{LnPd_{15}\}$ formation unlikely. The star-cube structure **1**, with its flexible water ligand coordination, demonstrates greater adaptability than either pure cube or star topologies, showing preference for Ce^{4+} and later lanthanides (Ln^{3+}). The chiral propeller cage **4** appears optimally suited for middle lanthanides (Ln^{3+}). These findings provide valuable insights for targeted synthesis of lanthanide-containing POPs with specific architectures. This proposal regarding size‑dependent structure selection is very preliminary. The current calculation suggests a trend, but additional systematic studies will be required to fully rationalize it.

3 Conclusions

This study successfully accomplished its primary objective of incorporating tetravalent cerium into anionic polyoxopalladate frameworks, leading to the discovery of three distinct lanthanide-containing POP architectures. The first represents a star-cube hybrid structure, $[CePd_{13}O_9(SeO_3)_9(H_2O)]^{6-}$, featuring a 10-coordinate Ce^{4+} centre within a unique half-cube/half-star geometry. The second, $[Ce_3Pd_{22}O_{16}(SeO_3)_{16}]^{8-}$, adopts a twisted dumbbell configuration comprising two lacunary $\{CePd_{11}\}$ units bridged by a central 8-coordinate Ce^{4+} ion. Additionally, we achieved the synthesis of axially chiral clusters $[LnPd_{12}O_7(SeO_3)_8Cl(H_2O)_2]^{4-}$ (Ln = Eu and Gd), which represent very rare examples of POPs with direct hetero anion coordination to the central lanthanide. The Ce^{4+}-containing POPs constitute some of the few known examples of tetravalent lanthanide incorporation in anionic frameworks, making them potentially valuable for applications in radioactive waste processing, organic synthesis, and catalysis. The chiral europium and gadolinium derivatives additionally open new possibilities in stereoselective chemistry.

Looking ahead, future investigations should pursue several important directions. First, comprehensive electrochemical characterization of the Ce-containing clusters would provide valuable insights into their redox behaviour. Direct use of Ce^{4+} salts in synthesis represents an important direction for future work. Second, developing methods for obtaining enantiomerically pure forms of the chiral compounds would be highly desirable. Third, systematic exploration of alternative capping groups (RXO_3^{n-}) could reveal new structure-directing effects. Fourth, detailed mechanistic studies would help elucidate the formation pathways and driving forces behind these architectures. Finally, examining the possibility of creating complete lanthanide series for each structure type would test the limits of this synthetic approach. These investigations promise to deepen our understanding of structure–property relationships in POP chemistry while enabling the rational design of functional materials with tailored characteristics.

Electronic Supplementary Material: Supplementary material (synthesis, X-ray-crystallography, structure description and bond valence sum calculations) is available in the online version of this article at https://doi.org/10.26599/POM.2026.9140137.

Data availability

All data needed to support the conclusions in the paper are presented in the manuscript and the Electronic Supplementary Material. Additional data related to this paper may be requested from the corresponding author upon request.

The X-ray crystallographic data have been deposited at the Crystallographic Data Center with codes CSD 2385249–2385253, which can be obtained free of charge via www.ccdc.cam.ac.uk./data_request/cif. Or by emailing data_request@ccdc.cam.ac.uk, or by contacting The Cambridge Crystallographic Data Centre, 12 Union Road, Cambridge CB2 1EZ, UK; fax: +44 1223 336033.

Acknowledgements

We gratefully acknowledge financial support from the EPSRC (Nos. EP/L023652/1, EP/R009902/1, EP/R020914/1, EP/R01308X/1, EP/S017046/1, EP/S019472/1, and EP/V048341/1), the European Research Council (Project 670467 SMART-POM) and the University of Glasgow. We thank the Diamond Light Source for machine time on Beamline I19 under the proposal CY30458.

Declaration of competing interest

There are no conflicts to declare. Author De-Liang Long is the advisory board member of this journal, but he is not involved in the peer-review or decision of this article.

Author contribution statement

Z. L. S: Data curation, validation, writing manuscript. V. L.: Data validation. D.-L. L.: Data curation, validation, writing manuscript, project team leader, funding acquisition. N. L. B.: Data validation, project team leader. L. C.: Project administration, funding acquisition, supervision. All the authors have approved the final manuscript.

Use of AI statement

None.

References

[1] Seechurn, C. C. C. J.; Kitching, M. O.; Colacot, T. J.; Snieckus, V. Palladium-catalyzed cross-coupling: A historical contextual perspective to the 2010 nobel prize. *Angew. Chem., Int. Ed.* **2012**, *51*, 5062–5085.

[2] Wang, D.; Weinstein, A. B.; White, P. B.; Stahl, S. S. Ligand-promoted palladium-catalyzed aerobic oxidation reactions. *Chem. Rev.* **2018**, *118*, 2636–2679.

[3] Yang, P.; Kortz, U. Discovery and evolution of polyoxopalladates. *Acc. Chem. Res.* **2018**, *51*, 1599–1608.

[4] Chubarova, E. V.; Dickman, M. H.; Keita, B.; Nadjo, L.; Miserque, F.; Mifsud, M.; Arends, I. W. C. E.; Kortz, U. Self-assembly of a heteropolyoxopalladate nanocube: $[Pd^{II}_{13}As^{V}_{8}O_{34}(OH)_6]^{8-}$. *Angew. Chem., Int. Ed.* **2008**, *47*, 9542–9546.

[5] Izarova, N. V.; Biboum, R. N.; Keita, B.; Mifsud, M.; Arends, I. W. C. E.; Jameson, G. B.; Kortz, U. Self-assembly of star-shaped heteropoly-15-palladate(II). *Dalton Trans.* **2009**, 9385–9387.

[6] Izarova, N. V.; Vankova, N.; Banerjee, A.; Jameson, G. B.; Heine, T.; Schinle, F.; Hampe, O.; Kortz, U. A noble-metalate bowl: The polyoxo-6-vanado(V)-7-palladate(II) $[Pd_7V_6O_{24}(OH)_2]^{6-}$. *Angew. Chem., Int. Ed.* **2010**, *49*, 7807–7811.

[7] Xu, F.; Miras, H. N.; Scullion, R. A.; Long, D. L.; Thiel, J.; Cronin, L. Correlating the magic numbers of inorganic nanomolecular assemblies with a $\{Pd_{84}\}$ molecular-ring Rosetta Stone. *Proc. Natl. Acad. Sci. USA* **2012**, *109*, 11609–11612.

[8] Yang, P.; Xiang, Y. X.; Lin, Z. G.; Bassil, B. S.; Cao, J.; Fan, L. Y.; Fan, Y. X.; Li, M. X.; Jiménez-Lozano, P.; Carbó, J. J. et al. Alkaline earth guests in polyoxopalladate chemistry: From nanocube to nanostar via an open-shell structure. *Angew. Chem., Int. Ed.* **2014**, *53*, 11974–11978.

[9] Zhao, Y.; Li, K. L.; Du, J.; Chen, C. Q.; Chen, S.; Yang, P. Binary heterogroup-templated scaffolds of polyoxopalladates as precatalysts for plasma-assisted ammonia synthesis. *ACS Appl. Mater. Interfaces* **2023**, *15*, 43899–43908.

[10] Ayass, W. W.; Miñambres, J. F.; Yang, P.; Ma, T.; Lin, Z. G.; Meyer, R.; Jaensch, H.; Bons, A. J.; Kortz, U. Discrete polyoxopalladates as molecular precursors for supported palladium metal nanoparticles as hydrogenation catalysts. *Inorg. Chem.* **2019**, *58*, 5576–5582.

[11] Long, D. L.; Tsunashima, R.; Cronin, L. Polyoxometalates: Building blocks for functional nanoscale systems. *Angew. Chem., Int. Ed.* **2010**, *49*, 1736–1758.

[12] Izarova, N. V.; Dickman, M. H.; Biboum, R. N.; Keita, B.; Nadjo, L.; Ramachandran, V.; Dalal, N. S.; Kortz, U. Heteropoly-13-palladates(II) $[Pd^{II}_{13}(As^{V}Ph)_8O_{32}]^{6-}$ and $[Pd^{II}_{13}Se^{IV}_{8}O_{32}]^{6-}$. *Inorg. Chem.* **2009**, *48*, 7504–7506.

[13] Scullion, R. A.; Surman, A. J.; Xu, F.; Mathieson, J. S.; Long, D. L.; Haso, F.; Liu, T. B.; Cronin, L. Exploring the symmetry, structure, and self-assembly mechanism of a gigantic seven-fold symmetric $\{Pd_{84}\}$ wheel. *Angew. Chem., Int. Ed.* **2014**, *53*, 10032–10037.

[14] Christie, L. G.; Surman, A. J.; Scullion, R. A.; Xu, F.; Long, D. L.; Cronin, L. Overcoming the crystallization bottleneck: A family of gigantic inorganic $\{Pd_x\}^{L}$ (x = 84, 72) palladium macrocycles discovered using solution techniques. *Angew. Chem., Int. Ed.* **2016**, *55*, 12741–12745.

[15] Bhattacharya, S.; Ma, X.; Mougharbel, A. S.; Haouas, M.; Su, P.; Espenship, M. F.; Taffa, D. H.; Jaensch, H.; Bons, A. J.; Stuerzer, T. et al. Discovery of a neutral 40-Pd^{II}-oxo molecular disk, $[Pd_{40}O_{24}(OH)_{16}\{(CH_3)_2AsO_2\}_{16}]$: Synthesis, structural characterization, and catalytic studies. *Inorg. Chem.* **2021**, *60*, 17339–17347.

[16] Xu, F.; Scullion, R. A.; Yan, J.; Miras, H. N.; Busche, C.; Scandurra, A.; Pignataro, B.; Long, D. L.; Cronin, L. A supramolecular heteropolyoxopalladate $\{Pd_{15}\}$ cluster host encapsulating a $\{Pd_2\}$ dinuclear guest: $[Pd^{II}_2\subset\{H_7Pd^{II}_{15}O_{10}(PO_4)_{10}\}]^{9-}$. *J. Am. Chem. Soc.* **2011**, *133*, 4684–4686.

[17] Yang, P.; Xiang, Y. X.; Lin, Z. G.; Lang, Z. L.; Jiménez-Lozano, P.; Carbó, J. J.; Poblet, J. M.; Fan, L. Y.; Hu, C. W.; Kortz, U. Discrete silver(I)-palladium(II)-oxo nanoclusters, $\{Ag_4Pd_{13}\}$ and $\{Ag_5Pd_{15}\}$, and the role of metal-metal bonding induced by cation confinement. *Angew. Chem., Int. Ed.* **2016**, *55*, 15766–15770.

[18] Barsukova, M.; Izarova, N. V.; Biboum, R. N.; Keita, B.; Nadjo, L.; Ramachandran, V.; Dalal, N. S.; Antonova, N. S.; Carbó, J. J.; Poblet, J. M. et al. Polyoxopalladates encapsulating yttrium and lanthanide ions, $[X^{III}Pd^{II}_{12}(AsPh)_8O_{32}]^{5-}$ (X = Y, Pr, Nd, Sm, Eu, Gd, Tb, Dy, Ho, Er, Tm, Yb, Lu). *Chem.—Eur. J.* **2010**, *16*, 9076–9085.

[19] Cardona-Serra, S.; Clemente-Juan, J. M.; Coronado, E.; Gaita-Ariño, A.; Camón, A.; Evangelisti, M.; Luis, F.; Martínez-Pérez, M. J.; Sesé, J. Lanthanoid single-ion magnets based on polyoxometalates with a 5-fold symmetry: The series $[LnP_5W_{30}O_{110}]^{12-}$ (Ln^{3+} = Tb, Dy, Ho, Er, Tm, and Yb). *J. Am. Chem. Soc.* **2012**, *134*, 14982–14990.

[20] Jia, X. D.; Jiang, J.; Liu, L. L.; Meng, L. N.; Chen, L. J.; Zhao, J. W. Two innovative fumaric acid bridging lanthanide-encapsulated hexameric selenotungstates containing mixed building units and electrochemical performance for detecting mycotoxin. *Inorg. Chem.* **2022**, *61*, 10965–10976.

[21] Ribó, E. G.; Bell, N. L.; Xuan, W. M.; Luo, J. C.; Long, D. L.; Liu, T. B.; Cronin, L. Synthesis, assembly, and sizing of neutral, lanthanide substituted molybdenum blue wheels $\{Mo_{90}Ln_{10}\}$. *J. Am. Chem. Soc.* **2020**, *142*, 17508–17514.

[22] Ribó, E. G.; Bell, N. L.; Long, D. L.; Cronin, L. Engineering highly reduced molybdenum polyoxometalates via the incorporation of d and f block metal ions. *Angew. Chem., Int. Ed.* **2022**, *61*, e202201672.

[23] Ruiz-Bilbao, E.; Pardo-Almanza, M.; Oyarzabal, I.; Artetxe, B.; San Felices, L.; García, J. A.; Seco, J. M.; Colacio, E.; Lezama, L.; Gutiérrez-Zorrilla, J. M. Slow magnetic relaxation and luminescent properties of mononuclear lanthanide-substituted keggin-type polyoxotungstates with compartmental organic ligands. *Inorg. Chem.* **2022**, *61*, 2428–2443.

[24] Iwano, T.; Shitamatsu, K.; Ogiwara, N.; Okuno, M.; Kikukawa, Y.; Ikemoto, S.; Shirai, S.; Muratsugu, S.; Waddell, P. G.; Errington, R. J. et al. Ultrahigh proton conduction via extended hydrogen-bonding network in a preyssler-type polyoxometalate-based framework functionalized with a lanthanide ion. *ACS Appl. Mater. Interfaces* **2021**, *13*, 19138–19147.

[25] Zhao, Y.; Li, C. L.; Chen, C. Q.; Du, J.; Kortz, U.; Gong, T.; Yang, P. Last piece of the puzzle: Lead-assisted assembly of an arsenopalladate nanostar as an antitumor metallodrug. *Inorg. Chem. Front.* **2024**, *11*, 1413–1422.

[26] Christie, L. G.; Asche, S.; Mathieson, J. S.; Vilà-Nadal, L.; Cronin, L. Investigating the formation of giant $\{Pd_{72}\}^{Prop}$ and $\{Pd_{84}\}^{Gly}$ macrocycles using NMR, HPLC, and mass spectrometry. *J. Am.*

Chem. Soc. **2018**, *140*, 9379–9382.
[27] Binnemans, K. Applications of tetravalent cerium compounds. *Handb. Phys. Chem. Rare Earths.* **2006**, *36*, 281–392.
[28] Colliard, I.; Nyman, M. Ce^{IV}_{70} oxosulfate rings, frameworks, supramolecular assembly, and redox activity. *Angew. Chem., Int. Ed.* **2021**, *60*, 7308–7315.
[29] Roy, L. E.; Ortiz-Acosta, D.; Batista, E. R.; Scott, B. L.; Blair, M. W.; May, I.; Del Sesto, R. E.; Martin, R. L. Luminescence in Ce^{IV} polyoxometalate $[Ce(W_5O_{18})_2]^{8-}$: A combined experimental and theoretical study. *Chem. Commun.* **2010**, *46*, 1848–1850.
[30] Iijima, J.; Ishikawa, E.; Nakamura, Y.; Naruke, H. Synthesis and structural investigation of sandwich polyoxotungstates containing cerium (III/IV) and mono-lacunary Keggin tungstophosphate units. *Inorg. Chim. Acta* **2010**, *363*, 1500–1506.
[31] Antonio, M. R.; Soderholm, L.; Williams, C. W.; Ullah, N.; Francesconi, L. C. Redox behavior of cerium in heteropolyoxotungstate complexes. *J. Chem. Soc. Dalton Trans.* **1999**, 3825–3830.
[32] Moons, J.; Van Rompuy, L. S.; Rodriguez, A.; Abdelhameed, S. A. M.; Simons, W.; Parac-Vogt, T. N. Hydrolysis of transferrin promoted by a cerium(IV)-Keggin polyoxometalate. *Polyhedron* **2019**, *170*, 570–575.
[33] Stroobants, K.; Moelants, E.; Ly, H. G. T.; Proost, P.; Bartik, K.; Parac-Vogt, T. N. Polyoxometalates as a novel class of artificial proteases: Selective hydrolysis of lysozyme under physiological pH and temperature promoted by a Cerium(IV) Keggin-type polyoxometalate. *Chem.—Eur. J.* **2013**, *19*, 2848–2858.
[34] Bhattacharya, S.; Barba-Bon, A.; Zewdie, T. A.; Müller, A. B.; Nisar, T.; Chmielnicka, A.; Rutkowska, I. A.; Schürmann, C. J.; Wagner, V.; Kuhnert, N. et al. Discrete, cationic palladium(II)-oxo clusters via f-metal ion incorporation and their macrocyclic host-guest interactions with sulfonatocalixarenes. *Angew. Chem., Int. Ed.* **2022**, *61*, e202203114.
[35] Abi-aad, E.; Bechara, R.; Grimblot, J.; Aboukais, A. Preparation and characterization of ceria under an oxidizing atmosphere. Thermal analysis, XPS, and EPR study. *Chem. Mater.* **1993**, *5*, 793–797.
[36] Ikeda-Ohno, A.; Tsushima, S.; Hennig, C.; Yaita, T.; Bernhard, G. Dinuclear complexes of tetravalent cerium in an aqueous perchloric acid solution. *Dalton Trans.* **2012**, *41*, 7190–7192.
[37] Demars, T. J.; Bera, M. K.; Seifert, S.; Antonio, M. R.; Ellis, R. J. Revisiting the solution structure of ceric ammonium nitrate. *Angew. Chem., Int. Ed.* **2015**, *54*, 7534–7538.
[38] Abellan, P.; Moser, T. H.; Lucas, I. T.; Grate, J. W.; Evans, J. E.; Browning, N. D. The formation of cerium(III) hydroxide nanoparticles by a radiation mediated increase in local pH. *RSC Adv.* **2017**, *7*, 3831–3837.
[39] Gagné, O. C.; Hawthorne, F. C. Comprehensive derivation of bond-valence parameters for ion pairs involving oxygen. *Acta Crystallogr. Sect. B: Struct. Sci. Cryst. Eng. Mater.* **2015**, *71*, 562–578.
[40] Spek, A. L. *PLATON* SQUEEZE: A tool for the calculation of the disordered solvent contribution to the calculated structure factors. *Acta Crystallogr. Sect. C: Struct. Chem.* **2015**, *71*, 9–18.
[41] Barsukova-Stuckart, M.; Izarova, N. V.; Jameson, G. B.; Ramachandran, V.; Wang, Z. X.; van Tol, J.; Dalal, N. S.; Biboum, R. N.; Keita, B.; Nadjo, L. et al. Synthesis and characterization of the dicopper(II)-containing 22-palladate(II) $[Cu^{II}_2Pd^{II}_{22}P^{V}_{12}O_{60}(OH)_8]^{20-}$. *Angew. Chem., Int. Ed.* **2011**, *50*, 2639–2642.
[42] Izarova, N. V.; Lin, Z. G.; Yang, P.; Kondinski, A.; Vankova, N.; Heine, T.; Kortz, U. The polyoxo-22-palladate(II), $[Na_2Pd^{II}_{22}O_{12}(As^{V}O_4)_{15}(As^{V}O_3OH)]^{25-}$. *Dalton Trans.* **2016**, *45*, 2394–2398.
[43] Ma, T.; Ma, X.; Lin, Z. G.; Zhang, J. Y.; Yang, P.; Csupász, T.; Tóth, I.; Misirlic-Dencic, S.; Isakovic, A. M.; Lembo, D. et al. Gallium(III)- and Thallium(III)-encapsulated polyoxopalladates: Synthesis, structure, multinuclear NMR, and biological activity studies. *Inorg. Chem.* **2023**, *62*, 13195–13204.
[44] Beaudoin, D.; Rominger, F.; Mastalerz, M. Synthesis and chiral resolution of C_3-symmetric tribenzotriquinacenes. *Eur. J. Org. Chem.* **2016**, *2016*, 4470–4472.
[45] Barsukova-Stuckart, M.; Izarova, N. V.; Barrett, R. A.; Wang, Z. X.; van Tol, J.; Kroto, H. W.; Dalal, N. S.; Jiménez-Lozano, P.; Carbó, J. J.; Poblet, J. M.; von Gernler, M. S. et al. Polyoxopalladates encapsulating 8-coordinated metal ions, $[MO_8Pd^{II}_{12}L_8]^{n-}$ (M = Sc^{3+}, Mn^{2+}, Fe^{3+}, Co^{2+}, Ni^{2+}, Cu^{2+}, Zn^{2+}, Lu^{3+}; L = $PhAsO_3^{2-}$, $PhPO_3^{2-}$, SeO_3^{2-}). *Inorg. Chem.* **2012**, *51*, 13214–13228.
[46] Lang, Z. L.; Yang, P.; Lin, Z. G.; Yan, L. K.; Li, M. X.; Carbó, J. J.; Kortz, U.; Poblet, J. M. Size and charge effect of guest cations in the formation of polyoxopalladates: A theoretical and experimental study. *Chem. Sci.* **2017**, *8*, 7862–7872.